EQUADIFF 10

Ivo Doležel; Pavel Šolín; Bohuš Ulrych
Fieldless methods for the simulation of stationary and nonstationary induction heating

Fieldless Methods for the Simulation of Stationary and Nonstationary Induction Heating

Ivo Doležel[1], Pavel Šolín[1] and Bohuš Ulrych[2]⋆

[1] Institute of Electrical Engineering of the ASCR,
Dolejškova 5, 18200 Prague, Czech Republic
Email: dolezel@iee.cas.cz
[2] Institute of Electrical Engineering of the ASCR,
Dolejškova 5, 18200 Prague, Czech Republic
Email: solin@iee.cas.cz
[3] Department of Electrical Engineering, Westbohemian University,
Sady pětatřicátníků 35, 30614 Pilsen, Czech Republic
Email: ulrych@kte.zcu.cz

Abstract. The paper gives a survey of a class of novel stationary and nonstationary methods for the simulation of the induction heating of nonferromagnetic metal bodies in harmonic electromagnetic fields. One of the main advantages of the presented method is the elimination of the surrounding air from the electromagnetic model, which strongly reduces the necessity of meshing and simplifies the computation. The task is formulated either as a stationary or as a non-stationary quasi-coupled problem, with respecting the temperature dependencies of all important material parameters. Distribution of the eddy currents and Joule losses in the metal body is solved by a system of second-kind Fredholm integral equations. Existence and uniqueness of solution for the continuos as well as discrete problem is shown. Convergence results for the numerical scheme are presented. The theoretical analysis is supplemented with examples motivated in the engineering practise..

This is the preliminary version of the paper.

1   Introduction

Mathematical modelling of the induction heating belongs to relatively well explored disciplines. The model consists of two second-order (generally non-linear) partial differential equations of the elliptic and/or parabolic types, whose solution yields distribution of the electromagnetic field, eddy currents, corresponding Joule losses and consequent temperature rise of the heated body. Sometimes, however, certain difficulties have to be overcome for obtaining correct results. We can mention, for example, the temperature dependent parameters of the materials involved, specific arrangements of the heaters etc. Nevertheless, in most geometries the field equations supplemented with correct boundary conditions may be solved by existing FEM-based professional programs (FLUX, ANSYS, MARC), and the results well correspond to the physical reality.

In case of thin metal slabs of negligible thickness or general three-dimensional metal bodies surrounded by (possibly moving) inductors of often very complicated shapes, the basic complication consists in the geometrical incommensurability of particular subregions in the investigated area (geometry of the metal body versus 3D inductor and/or practically unbounded air). Using methods such as FEM can lead to serious problems associated with generation of the discretisation grid that may result in unacceptable errors occurring particularly at the electromagnetic field calculation.

The paper offers an alternative method for direct determining the local Joule losses (that represent the input data for the consequent thermal calculation) based on solution of a system of second-kind Fredholm integral equations for the eddy current density in the metal body. Detailed knowledge of the 3D electromagnetic field is, therefore, unnecessary (here the atribute *fieldless* of the proposed method is originated) and the mentioned problems are avoided. The temperature field distribution is then solved by means of the non-stationary heat transfer equation with a special procedure for correcting values of the temperature dependent material properties.

2   Heating of thin non-ferromagnetic metal slabs (2D case)

A thin non-ferromagnetic slab Ω_1 of sizes a, b and h is heated by an inductor formed by two equal coils Ω_2 and Ω_2'. positioned symmetrically with respect to the plate (Fig. 1). Both coils carrying identical harmonic currents I_{ext} and I_{ext}' of angular frequency ω produce a field perfectly perpendicular to the slab. Thickness h of the slab is very small with respect to the other measures, so that the electromagnetic quantities may be considered independent of co-ordinate y. The inductor contains no ferromagnetic parts.

Due to absence of non-linearities within the investigated domain all quantities of the electromagnetic field may be expressed in terms of their phasors.
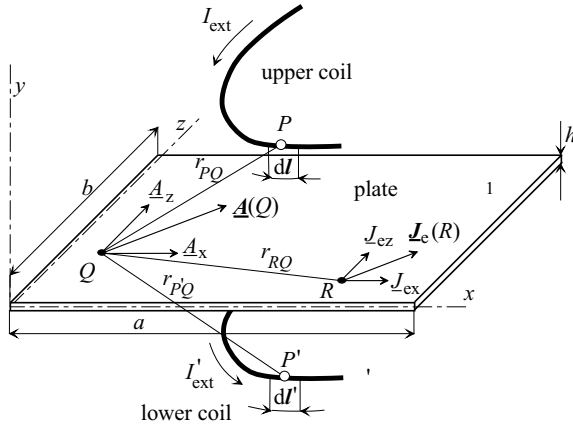
Fig. 1. The investigated arrangement

3   The coupled electromagnetic-thermal model (2D case)

Let Q be a point within the slab lying in plane $y = 0$. Phasor $\underline{\boldsymbol{A}}$ of the vector potential at this point is given by superposition of three components excited by the field currents I_{ext} and I'_{ext} and the eddy currents in the slab

$$\underline{\boldsymbol{A}}(Q) = \underline{\boldsymbol{A}}(PQ) + \underline{\boldsymbol{A}}(P'Q) + \underline{\boldsymbol{A}}(RQ) =$$

$$= \frac{\mu_0}{4\pi} \left(\underline{I}_{\text{ext}} \int_{\Omega_2} \frac{\mathrm{d}\boldsymbol{l}(P)}{r_{PQ}} + \underline{I}'_{\text{ext}} \int_{\Omega'_2} \frac{\mathrm{d}\boldsymbol{l}'(P')}{r_{P'Q}} + \int_{\Omega_1} \frac{\underline{\boldsymbol{J}}_{\text{eddy}}(R)}{r_{RQ}} \mathrm{d}V \right) =$$

$$= \frac{\mu_0}{4\pi} \left(\underline{I}_{\text{ext}} \int_{\Omega_2} \frac{\mathrm{d}\boldsymbol{l}(P)}{r_{PQ}} + \underline{I}'_{\text{ext}} \int_{\Omega'_2} \frac{\mathrm{d}\boldsymbol{l}'(P')}{r_{P'Q}} + \iint_S \frac{\underline{\boldsymbol{J}}_{\text{eddy}}(R)}{r_{RQ}} h \mathrm{d}S \right). \qquad (1)$$

Here, μ_0 denotes the permeability of vacuum, $\mathrm{d}\boldsymbol{l}$ and $\mathrm{d}\boldsymbol{l}'$ are vectors denoting the elementary lengths of conductors of the field coils, $\mathrm{d}V$ the elementary volume of the slab and S the cross-section of the slab in plane $y = 0$. All remaining symbols follow from Fig. 1.

Phasors $\underline{\boldsymbol{A}}(PQ)$ and $\underline{\boldsymbol{A}}(P'Q)$ have generally three components, according to the shape of the coil. In our case these components in direction x are equal, in direction z as well, and components in direction y eliminate one another. Equation (1) may be now rewritten as follows

$$\underline{\boldsymbol{A}}(Q) = \frac{\mu_0}{4\pi} \left(2\underline{I}_{\text{ext}} \int_{\Omega_2} \frac{\mathrm{d}\boldsymbol{l}(P)}{r_{PQ}} + h \int_{\Omega_1} \frac{\underline{\boldsymbol{J}}_{\text{eddy}}(R)}{r_{RQ}} \mathrm{d}S \right). \qquad (2)$$

For the next considerations it is useful to express vector potential $\boldsymbol{A}(Q)$ in the slab in terms of the eddy current density $\boldsymbol{J}_{\text{eddy}}(Q)$. Starting from the second

Maxwell equation

$$\mathrm{rot}\boldsymbol{E} = -\frac{\partial \boldsymbol{B}}{\partial t} = -\frac{\partial \mathrm{rot}\boldsymbol{A}}{\partial t} \tag{3}$$

and interchanging the order of the operators we get

$$\boldsymbol{E} = -\frac{\partial \boldsymbol{A}}{\partial t} - \mathrm{grad}\varphi, \tag{4}$$

where φ denotes the scalar potential. Applying this equation to the slab that is not connected to any external source of voltage ($\varphi = 0$) and rewriting it in terms of the corresponding phasor quantities we finally obtain

$$\underline{\boldsymbol{E}} = -\mathrm{j}\omega\underline{\boldsymbol{A}} \Rightarrow \underline{\boldsymbol{J}}_{\mathrm{eddy}} = -\mathrm{j}\omega\gamma\underline{\boldsymbol{A}}. \tag{5}$$

Hence, using the symbolics from (1),

$$\underline{\boldsymbol{A}}(Q) = \frac{\mathrm{j}}{\omega\gamma}\underline{\boldsymbol{J}}_{\mathrm{eddy}}(Q), \tag{6}$$

where γ denotes the electrical conductivity of the slab and ω the angular frequency of the field currents I_{ext} (I'_{ext}). Substitution of (6) into (2) provides the basic integral equation for $\underline{\boldsymbol{J}}_{\mathrm{eddy}}$

$$\mathrm{j}\underline{\boldsymbol{J}}_{\mathrm{eddy}}(Q) - \kappa_1 \int_S \frac{\underline{\boldsymbol{J}}_{\mathrm{eddy}}(R)}{r_{RQ}}\mathrm{d}S = \kappa_2 \underline{\boldsymbol{I}}_{\mathrm{ext}} \int_{\Omega_2} \frac{\mathrm{d}\boldsymbol{l}(P)}{r_{PQ}}, \tag{7}$$

where

$$\kappa_1 = \frac{\omega\gamma\mu_0 h}{4\pi}, \qquad \kappa_2 = \frac{\omega\gamma\mu_0}{2\pi}.$$

This phasor equation may easily be subdivided into two equations (for the components in directions x and z) of the complex character.

The specific average Joule losses w_{Ja} in the metal body are then given by formula

$$w_{\mathrm{Ja}} = \frac{\underline{\boldsymbol{J}}_{\mathrm{eddy}} \cdot \underline{\boldsymbol{J}}_{\mathrm{eddy}}^*}{\gamma}, \tag{8}$$

where $\underline{\boldsymbol{J}}_{\mathrm{eddy}}^*$ is the complex conjugate to $\underline{\boldsymbol{J}}_{\mathrm{eddy}}$. The non-stationary distribution of the temperature in the metal body is generally described (for example [2]) by equation

$$\mathrm{div}(\lambda\,\mathrm{grad}\,T) = \rho c\frac{\partial T}{\partial t} - w_{\mathrm{Ja}}, \tag{9}$$

where λ denotes the thermal conductivity, ρ the specific mass of the heated material, c its specific heat and w_{Ja} the specific Joule losses given by (8). The boundary condition along the whole surface of the body reads (radiation is not considered)

$$-\lambda\frac{\partial T}{\partial n} = \alpha(T - T_{\mathrm{ext}}), \tag{10}$$

where α denotes the coefficient of the convective heat transfer, T_{ext} the temperature of the surrounding medium (moving or quiet air) and n direction of the outward normal.

As this simpler 2D case is analogous to the next (slightly more complex) 3D one concerning the discretization, analysis of solvability and uniqueness both of the continuous and discrete problem and also concerning the convergence of the numerical scheme, we shall perform these considerations only for the three-dimensional model.

4   Heating of non-ferromagnetic metal bodies (3D case)

A bounded metal body Ω_1 with a Lipschitz-continuous boundary is heated by an inductor formed by a system of conductors and/or coils Ω_2 (Fig. 2). For simplicity, let the conductors and coils carry identical harmonic current I_{ext} of angular frequency ω. The inductor contains no ferromagnetic parts.
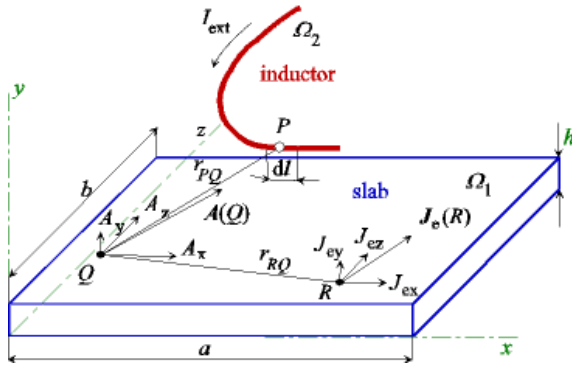

Fig. 2. The investigated arrangement

Due to absence of non-linearities within the investigated domain all quantities of the electromagnetic field may be expressed in terms of their phasors.

5   The coupled electromagnetic-thermal model (3D case)

Let $Q \in \Omega_1$. Phasor $\underline{\boldsymbol{A}}$ of the vector potential at this point is given by superposition of two components excited by the field currents I_{ext} and the eddy currents $\underline{\boldsymbol{J}}_{\text{eddy}}$ in Ω_1:

$$\underline{\boldsymbol{A}}(Q) = \underline{\boldsymbol{A}}(PQ) + \underline{\boldsymbol{A}}(RQ) = \frac{\mu_0}{4\pi}\left(\underline{I}_{\text{ext}}\int_{\Omega_2}\frac{\mathrm{d}\boldsymbol{l}(P)}{r_{PQ}} + \int_{\Omega_1}\frac{\underline{\boldsymbol{J}}_{\text{eddy}}(R)}{r_{RQ}}\mathrm{d}V\right). \quad (11)$$

Similarly as in the previous case, the second Maxwell equation yields

$$\underline{\boldsymbol{A}}(Q) = \frac{\mathrm{j}}{\omega\gamma}\underline{\boldsymbol{J}}_{\mathrm{eddy}}(Q) \tag{12}$$

where γ denotes the electrical conductivity of the metal and ω the angular frequency of the field currents I_{ext}. Substitution of (12) into (11) provides the basic integral equation for $\underline{\boldsymbol{J}}_{\mathrm{eddy}}$

$$\mathrm{j}\,\underline{\boldsymbol{J}}_{\mathrm{eddy}}(Q) - \kappa \int_{\Omega_1} \frac{\underline{\boldsymbol{J}}_{\mathrm{eddy}}(R)}{r_{RQ}}\mathrm{d}V = \kappa\,\underline{\boldsymbol{I}}_{\mathrm{ext}} \int_{\Omega_2} \frac{\mathrm{d}\boldsymbol{l}(P)}{r_{PQ}} \tag{13}$$

where $\kappa = \omega\gamma\mu_0 h/(4\pi)$. Here, μ_0 denotes the permeability of vacuum, $\mathrm{d}\boldsymbol{l}$ and $\mathrm{d}\boldsymbol{l}'$ are vectors denoting the elementary lengths of conductors of the field coils and $\mathrm{d}V$ the elementary volume of Ω_1. All remaining symbols follow from Fig. 2.

Coupling with the heat transfer equation occurs in the same way as in the previous case, using Joule losses as source terms.

The system (13) is discretized (see also [3]) using a first-order collocation scheme based on a discretitation of Ω_1 with piecewise linear approximation of all components of $\underline{\boldsymbol{J}}_{\mathrm{eddy}}$ in each cell. The only difficulty is with the diagonal coefficients of the corresponding matrix that are given by improper integrals. Their values are, however, finite and may be, with some effort, determined analytically. The arising dense system of linear equations can be solved e.g. by the Gauss elimination. The heat transfer equation (9) (formally the same in the 2D and 3D case) is semi-discretized in space using the method of lines and integrated in time using higher-order explicit Runge-Kutta schemes. Temperature-dependent material parameters are adjusted automatically during the time-evolution.

6   Analysis of solvability and uniqueness (3D case)

The phasor equation (13) may easily be subdivided into three identical equations (for the components in spatial directions x, y, z) of a complex form. For the x-component, we obtain

$$\mathrm{j}\,\underline{J}_{\mathrm{eddy,x}}(Q) - \kappa \int_{\Omega_1} \frac{\underline{J}_{\mathrm{eddy,x}}(R)}{r_{RQ}}\mathrm{d}V = \kappa\,\underline{I}_{\mathrm{ext}} \int_{\Omega_2} \frac{\mathrm{d}x(P)}{r_{PQ}}. \tag{14}$$

Using a substitution

$$\boldsymbol{L}_{\mathrm{x}}(\boldsymbol{v}) = \left(\frac{-\mathrm{Im}\{\underline{J}_{\mathrm{eddy,x}}\}}{\kappa}, \frac{\mathrm{Re}\{\underline{J}_{\mathrm{eddy,x}}\}}{\kappa} \right)^{T}(\boldsymbol{v}), \tag{15}$$

$$\boldsymbol{F}_{\mathrm{x}}(\boldsymbol{v}) = \int_{\Omega_2} \frac{\mathrm{d}x}{|\boldsymbol{u}-\boldsymbol{v}|} \left(\mathrm{Re}\{\underline{I}_{\mathrm{ext}}\}, \mathrm{Im}\{\underline{I}_{\mathrm{ext}}\} \right)^{T}, \tag{16}$$

we can rewrite (14) into an operator form

$$(\boldsymbol{I} + \boldsymbol{K})\boldsymbol{L}_{\mathrm{x}} = \boldsymbol{F}_{\mathrm{x}} \tag{17}$$

with

$$(\boldsymbol{K}\boldsymbol{L}_{\mathrm{x}})(\boldsymbol{v}) = \int_{\Omega_1} \boldsymbol{k}(\boldsymbol{v}, \boldsymbol{w})\boldsymbol{L}_{\mathrm{x}}(\boldsymbol{w})\mathrm{d}\boldsymbol{w}, \tag{18}$$

$$\boldsymbol{k}(\boldsymbol{v}, \boldsymbol{w}) = \frac{\kappa}{|\boldsymbol{v} - \boldsymbol{w}|}\boldsymbol{M}, \quad \boldsymbol{M} = \begin{pmatrix} 0 & -1 \\ 1 & 0 \end{pmatrix}. \tag{19}$$

It is easy to see that the operator $\boldsymbol{K} \colon C(\Omega_1) \to C(\Omega_1)$ is compact and self adjoint in a weighted $L^2(\Omega_1)$-norm with a weighting factor $1/\kappa$. Therefore, under a technical assumption – let us denote it by (A_{-1}) – that the homogeneous equation $(\boldsymbol{I} + \boldsymbol{K})\boldsymbol{L}_{\mathrm{x}} = 0$ has only trivial solution (i.e. -1 is not an eigenvalue of $\boldsymbol{K}$), the Fredholm alternative immediately yields the solvability, uniqueness and continuous dependence on the right-hand-side for (17). An analogous conclusion holds, of course, for the remaining spatial components. Let us remark that the assumption (A_{-1}) is obviously satisfied from the physical point of view. However, its correct mathematical proof exhibits some difficulties and is still in progress.

There are no problems with the existence and uniqueness of solution for the parabolic heat transfer equation (9) in a weak sense as all the temperature-dependent material parameters are Lipschitz-continuous functions.

Analysis of the solvability and uniqueness of the discrete problem is performed in an analogous way.

7   Convergence of the numerical scheme (3D case)

Let us consider the continuous problem (17). For simplicity, let us further consider that the domain Ω_1 is covered by the discretization mesh exactly ($\Omega_{1,h} \equiv \Omega_1$). With a function κ_h obtained by elementwise averaging the function κ from (14), we can write the discrete problem for the eddy currents $\underline{\boldsymbol{J}}_{\mathrm{eddy}}$ in Ω_1 as

$$(\boldsymbol{I} + \boldsymbol{K}_h)\boldsymbol{L}_{\mathrm{x},h} = \boldsymbol{F}_{\mathrm{x},h}. \tag{20}$$

with

$$(\boldsymbol{K}_h\boldsymbol{L}_{\mathrm{x},h})(\boldsymbol{v}) = \int_{\Omega_1} \boldsymbol{k}_h(\boldsymbol{v}, \boldsymbol{w})\boldsymbol{L}_{\mathrm{x},h}(\boldsymbol{w})\mathrm{d}\boldsymbol{w}, \tag{21}$$

$$\boldsymbol{k}_h(\boldsymbol{v}, \boldsymbol{w}) = \frac{\kappa_h}{|\boldsymbol{v} - \boldsymbol{w}|}\boldsymbol{M}, \quad \boldsymbol{M} = \begin{pmatrix} 0 & -1 \\ 1 & 0 \end{pmatrix}. \tag{22}$$

Subtracting (20) from (17) we obtain that $\boldsymbol{L}_{\mathrm{err}} = \boldsymbol{L}_{\mathrm{x}} - \boldsymbol{L}_{\mathrm{x},h}$ is governed by

$$\boldsymbol{L}_{\mathrm{err}} = (\boldsymbol{I} + \boldsymbol{K})^{-1}\left[\boldsymbol{F}_{\mathrm{err}} - (\boldsymbol{K} - \boldsymbol{K}_h)\boldsymbol{L}_{\mathrm{x},h}\right] \tag{23}$$

where obviously $\boldsymbol{F}_{\mathrm{err}} = \boldsymbol{F}_{\mathrm{x}} - \boldsymbol{F}_{\mathrm{x},h} \to 0$ as the grid diameter $h \to 0$, $\boldsymbol{K} - \boldsymbol{K}_h \to 0$ as $h \to 0$ from the definition of κ_h and $\boldsymbol{L}_{\mathrm{x},h}$ is bounded from the compactness of $(\boldsymbol{I} + \boldsymbol{K}_h)^{-1}$. Note that again we used the technical assumption (A_{-1}) from the previous section together with a similar assumption $(A_{-1,h})$ for the discrete problem.

Finally, convergence in the source terms of the heat transfer equation (9) yields also the convergence of the whole discrete coupled model for all finite times. Obviously, when integrating explicitly in time one has to fulfil the classical stability condition for the time step $\triangle t \in O(h^2)$ for parabolic equation.

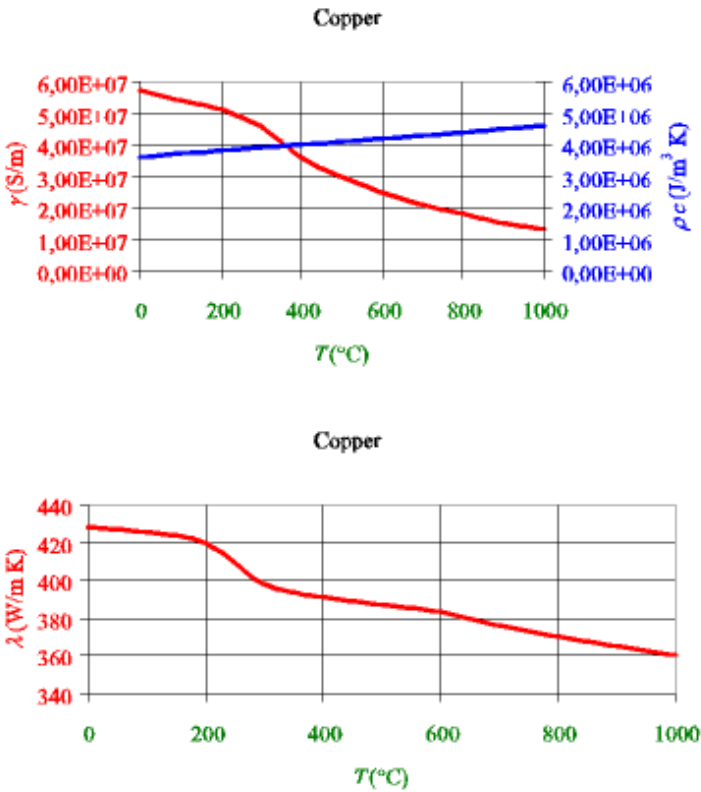## 8   Example: Temperature-Dependent Material Parameters for Copper

Fig. 3. Temperature-dependent γ, λ and ρc for copper

9   Example 1: Heating of a thin copper plate

The suggested methodology has been applied to an arrangement depicted in Fig. 4. A copper slab of sizes 0.3×0.6 m was heated by two helicoidal inductors (number of turns $N = 10$) of the indicated geometry.
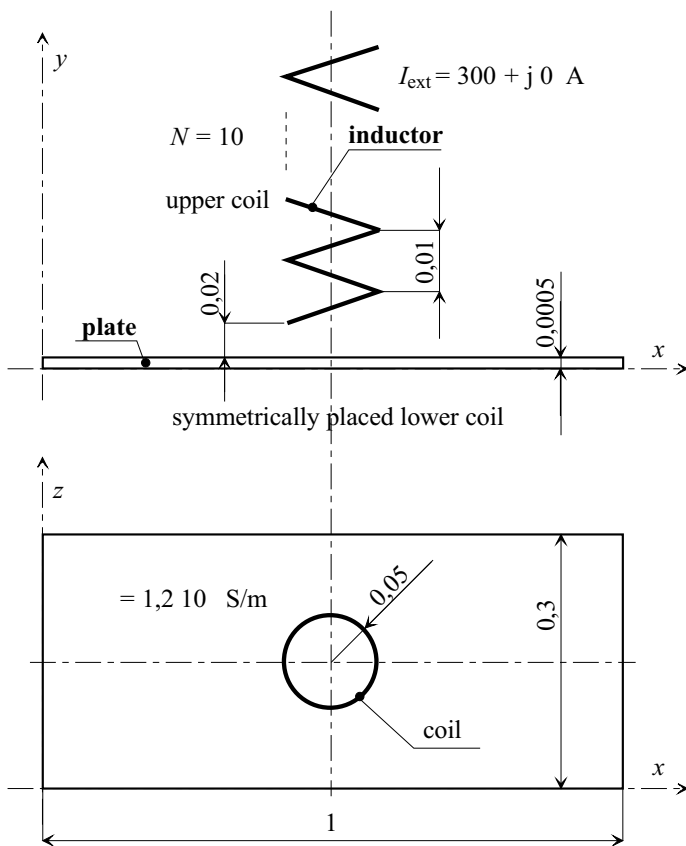
Fig. 4. The investigated arrangement

The dependencies of parameters γ and λ on temperature T have been shown in Fig. 3. The temperature dependence of product ρc is considered linear: $\rho c = 3.6312 \cdot 10^6 + 934.5 \cdot (T - 20)$ J/deg m^3. Parameter $\alpha = 25$ W/m^2 deg and $T_{ext} = 20$ °C. All numerical computations have been performed by a special user program package developed by the authors and written in C++.

Several results for parameters $f = 1000$ Hz and $h = 0.0005$ m are shown in Figs. 5 to 7. Fig. 5 depicts the distribution of the temperature (at various time

levels) in the slab along line $z = 0.05\,\mathrm{m}$ and Fig. 6 the same distribution along line $z = 0.15\,\mathrm{m}$. Fig. 7 shows the time evolution of temperature T at the "hottest" point of the slab (co-ordinates $0.25\,\mathrm{m}$ and $z = 0.15\,\mathrm{m}$).
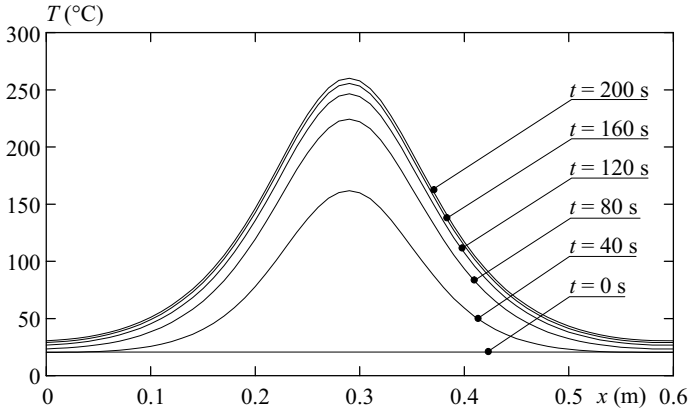

Fig. 5. Distribution of temperature along line $z = 0.05\,\mathrm{m}$
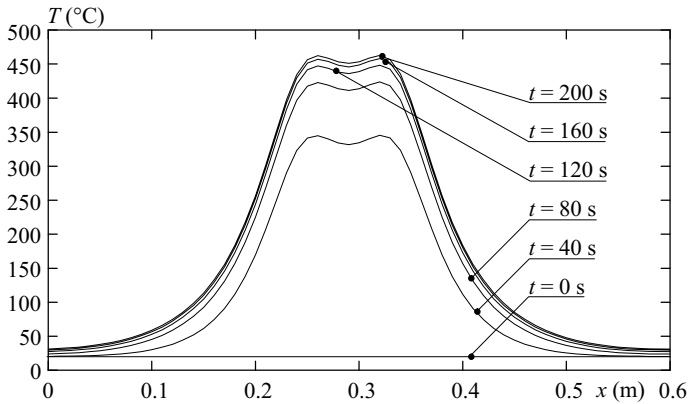
Fig. 6. Distribution of temperature along line $z = 0.15\,\mathrm{m}$
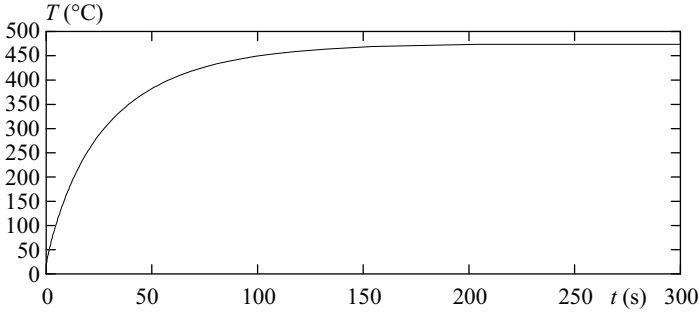
Fig. 7. Evolution of the temperature at point $[0.25, 0.15]$ m

10   Example 2: Heating of a brass prism

A prismatic brass bar (Fig. 8) is heated by a coil-shaped inductor formed by a hollow tubular water-cooled conductor.

The basic arrangement of the system is obvious from parts **A** and **B** of Fig. 8. The field current in the inductor $I = 550$ A, its frequency $f = 150$ kHz. As the inductor is formed by a massive conductor, it was substituted by 8 thinner conductors located at points indicated in part **C** of Fig. 8. Each of these conductors carries current $I_k = 68.75$ A, $k = 1, 2, ..., 8$.

The starting temperature T_{start} of the body and temperature T_{ext} of the surrounding air is 20 °C. Coefficient of the convective heat transfer is 25 W/m^2. The discretisation grid covering the body consists of 750 cubic elements sized $5 \times 5 \times 5$ mm.

In the following Fig. 9 we present a series of color plots for the temperature evolution in the investigated metal body. The Fig. 10 shows steady-state temperature cutlines at the time $t = 90$ min corresponding to its axis and to one of its longest edges.
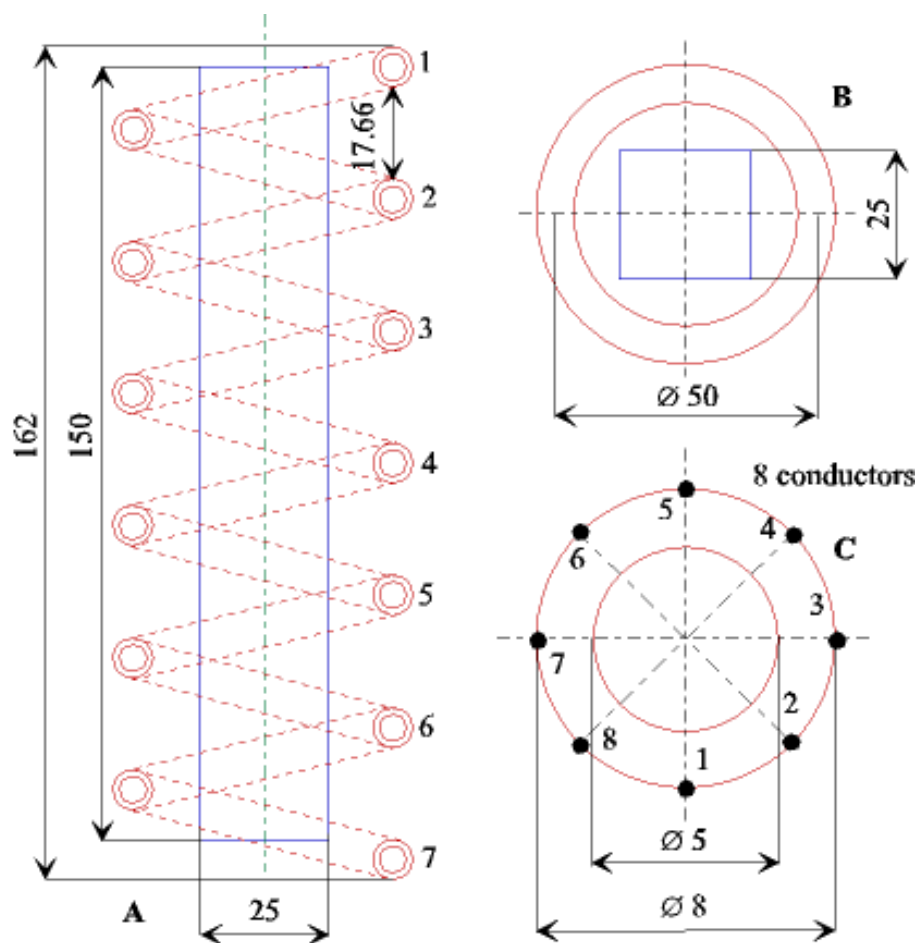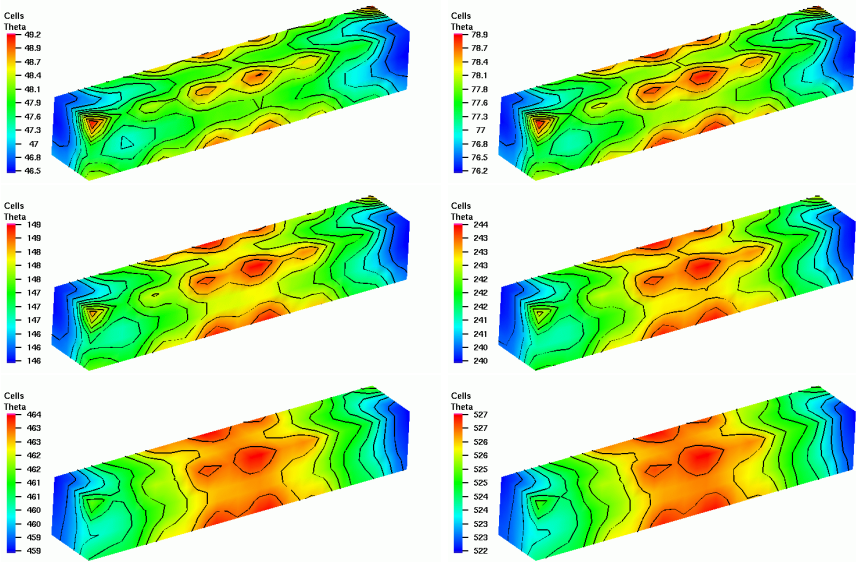
Fig. 8. The investigated arrangement

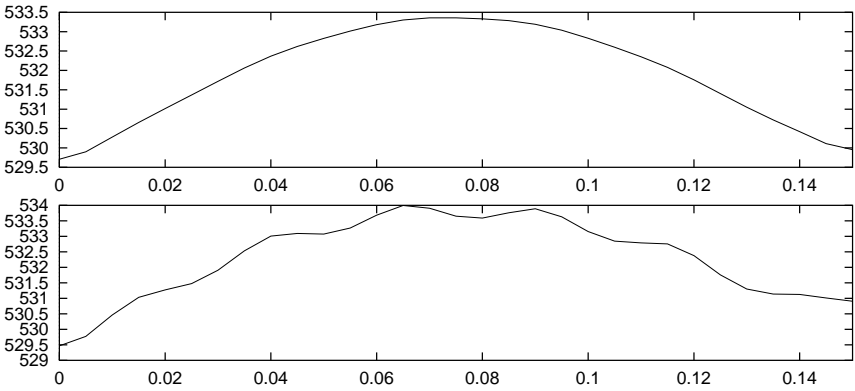**Fig. 9.** Temperature distribution after 1, 2, 5, 10, 30 and 60 minutes.

Fig. 10. Temperature cutlines after 90 minutes of heating (axis and edge).

11   Example 3: Heating of a brass frame

In this section we present another example related to the induction heating of a brass frame. The outer measures of the frame are $25 \times 25 \times 150$ mm. Its geometry and the discretization grid consisting of cubic elements sized $1 \times 1 \times 1$ mm are shown in Fig. 11. The inductor is formed by a single coil with $N = 6$ turns, radius $r = 19$ mm, which carries a harmonic current $I = 500$ A of frequency $f = 2000$ Hz. The length-increment corresponding to one turn of the coil is $\triangle l = 13$ mm. Remaining parameters are the same as in the previous example.
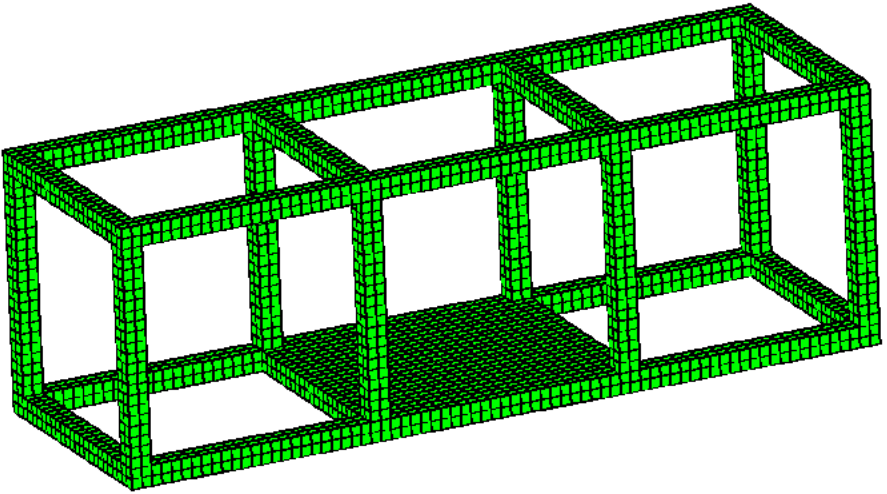

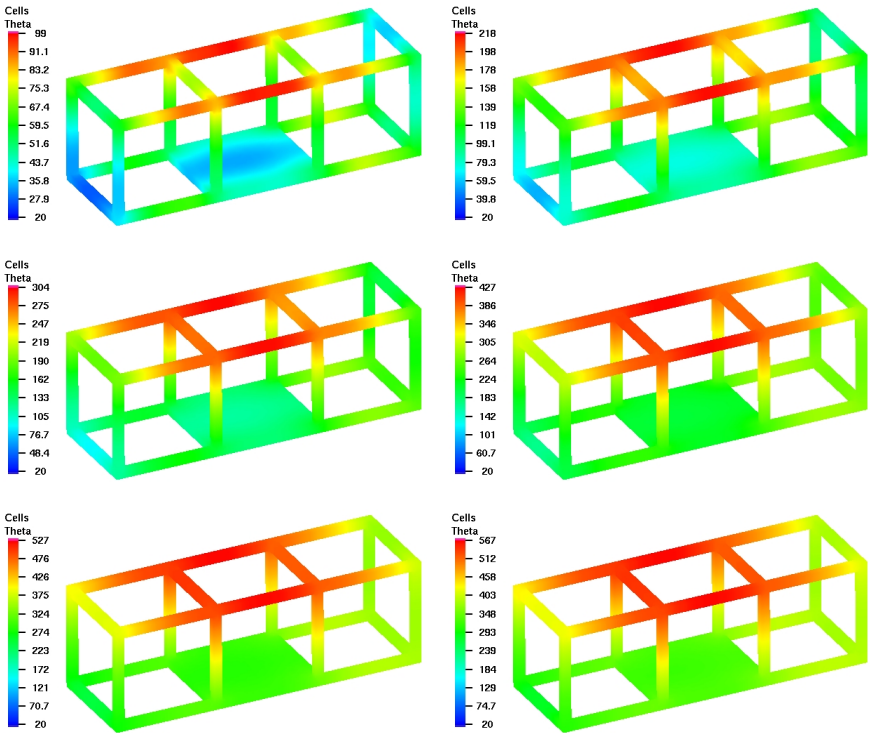**Fig. 11.** Brass frame, geometry and mesh.

Fig. 12. Temperature distribution after 1, 3, 5, 9, 13, 15 seconds.

The Fig. 12 shows the temperature evolution during the first 15 seconds of the heating. After approximately 15 seconds, the steady state is reached The reader may notice that in this case the temperature distribution is not uniform (as e.g. in the last example), which may indicate that, from the engineering point of view, the inductor may undergo some additional re-arrangements.

References

1. Engl, H. W., Integralgleichungen (Springer, Wien, 1997, in German).
2. Lykov, A. V., Theory of Heat Conduction (Moscow, 1967, in Russian).
3. Šolín, P., Doležel, I., Škopek, M., Ulrych, B., Stationary Temperature Field in a Non-magnetic Thin Plate Heated by Transversal Electromagnetic Field, Acta Technica CSAV 45 (2000) 105–128.